Available online at www.sciencedirect.com
SCIENCE DIRECT®
International Journal of Heat and Mass Transfer 49 (2006) 297–306
International Journal of HEAT and MASS TRANSFER
www.elsevier.com/locate/ijhmt

The effects of plasma characteristics on the melting time at the front surface of a film on a substrate: An exact solution

F.B. Yeh *

Department of Marine Mechanical Engineering, Chinese Naval Academy, P.O. Box 90175, Tsoying, 813, Kaohsiung, Taiwan, ROC

Received 3 February 2005; received in revised form 22 June 2005
Available online 24 August 2005

Abstract

Plasma heating of a film on a substrate is solved by using the Laplace transform method. The plasma is composed of a collisionless presheath and sheath on an electrically negative bias film partially reflecting and secondly emitting ions and electrons. The heating of the film from the plasma accounting for the presheath and sheath is determined from the kinetic analysis. This work proposes an analytical model to calculate the melting time and heating rate of the front surface of a film on the substrate, and provides quantitative results applicable to control the temperature evolution and the melting time in the film. The predicted surface temperature of the film on the substrate as a function of time is found to agree well with experimental data. The effects of dimensionless bias voltage, reflectivities of the ions and electrons on the wall, electron-to-ion source temperature ratio at the presheath edge, ion-to-electron mass ratio, charge number, plasma flow work-to-heat conduction ratios, substrate-to-film solid thermal conductivity ratios, and film-to-substrate solid specific heat ratios on the melting time and heating rate of the front surface are obtained. The contact Biot number between the film and substrate to simulate the heat conduction into substrate is also discussed. The results show that the melting time is strongly dependent on the plasma parameters and thermal properties of the material.

Keywords: Plasma energy flux; Sheath; Presheath; Negative bias voltage; Melting time; Heating rate

1. Introduction

Plasma etching, spray deposition, sputtering, cutting, surface treatment, and nuclear fusion devices, etc. are controlled by energy transfer from the plasma to surfaces. When a plasma is in contact with a workpiece surface, a thin layer called the sheath or space-charge region exists on the wall [1]. The presheath ($\sim 10^{-4}$ m), which lies between the bulk plasma and sheath, is an ionization region to supply the ions lost to the wall and accelerates the ions up to and beyond sonic speed before entering the sheath, as first explicitly pointed out by Bohm [2]. Heat transport in the workpiece is determined by the plasma energy transfer, which is controlled by the parameters such as the charge number, mass and temperature ratios of the ions and electrons generated in the presheath, and properties of the wall, etc. Several plasma-based techniques may be employed

* Tel./fax: +886 7 583 4861.
E-mail address: fbyeh@mail.cna.edu.tw

0017-9310/$ - see front matter © 2005 Elsevier Ltd. All rights reserved.
doi:10.1016/j.ijheatmasstransfer.2005.06.024

Nomenclature

B	defined in Eq. (18)
Bi	Biot number, $Bi = h_\infty s/k_f$, $Bi_a = h_a s/k_f$, $Bi_c = h_c s/k_f$
C_p	specific heat
C_{pfs}	the ratio of specific heat, $C_{pfs} = c_{pf}/c_{ps}$
D	Dawson function
e	electron charge
E_i	dimension and dimensionless ionization energy, $E_i = E_i/k_B T_{e0}$
h	heat transfer coefficient
j	dimension and dimensionless current density, $j = j/en_{e0}(K_B T_{e0}/m_i)^{1/2}$
k	solid thermal conductivity
k_B	Boltzmann constant
K_{sf}	substrate-to-film solid thermal conductivity ratio, $K_{sf} = k_s/k_f$
m	particle mass
M	ion-to-electron mass ratio, $M = m_i/m_e$
n	particle density
Q	dimension and dimensionless total energy flux $Q = Q/[n_{e0}k_B T_{e0}(k_B T_{e0}/m_i)^{1/2}]$
s	the thickness of thin film
t	time
T	temperature
x	Cartesian coordinate
Z_i	charge number

Greek symbols

Θ	plasma flow work-to-thermal conduction ratio, $\Theta = n_{e0}k_B T_{e0}(k_B T_{e0}/m_i)^{1/2}/(k_f T_\infty/s)$
ε	defined in Eq. (18)
λ	dimensionless temperature, $\lambda = (T - T_\infty)/T_\infty$
α	dimensionless thermal diffusivity
ξ	dimensionless coordinate, $\xi = x/s$
φ	dimension and dimensionless work function, $\varphi = \varphi/k_B T_{e0}$
κ	electron-to-ion source temperature ratio at presheath edge, $\kappa = T_{e0}/T_{i0}$
γ	reflectivity
ρ	density
ρ_{fs}	the ratio of density, $\rho_{fs} = \rho_f/\rho_s$
τ	dimensionless time, $\tau = k_f t/\rho_f c_{pf} s^2$
ϕ, χ	dimensional and dimensionless potential, $\chi = -e\phi/k_B T_{e0}$
Ω, Ω_{1b}	functions, defined in Eqs. (2) and (4), respectively

Subscripts

b	boundary between sheath and presheath
bias	negative bias voltage
e, i	electron and ion
f	floating condition or a film
ff	finite film
m	melting
s	substrate
tot	total
w	wall
0, 0′	coordinate origin at $\phi = 0$ and $\xi = 0$, respectively, as shown in Fig. 1

to control energy and mass fluxes of the ions and electrons. For example, the application of a direct current (DC) bias or radio frequency (RF) bias can be used to accelerate the ions and retard the electrons from the plasma to the surface.

Thermal conditions at the workpiece surface play an important role in plasma–wall interactions. They strongly affect elementary processes, such as adsorption, desorption, diffusion, and chemical processes in semiconductor manufacturing and the lifetime of plasma facing materials in fusion devices. Especially in the case of thin film deposition, the structure and morphology of the layers depend sensitively on the thermal conditions at the surface. The surface temperature is strongly influenced by the plasma energy, due to energetic particle bombardment. Over the past decades there has been intensive research to study energy transport encountered in the cathode or near wall region of electric arc discharges, lamps, fusion devices, edge plasmas, ion implantation, deposition, etching, etc. [3–11]. Predictions of melting time, heating rate at the front surface and temperature distributions in a workpiece in contact with the plasma as functions of plasma characteristics and thermal properties of workpieces are still incomplete [12–16].

The aim of the present work is to solve the plasma heating of a film on a substrate by using the Laplace integral transform method. The film experiences heating induced by energy flux coming from the bulk plasma through the presheath and sheath to the surface, based on the analysis from a previous work [4]. In this study, a one-dimensional unsteady heat conduction model is developed to systematically predict unsteady temperature distributions in the film and substrate, and calculate the melting time and heating rate of the front surface of the film on the substrate subject to a negative bias voltage. The effects of the plasma characteristics and properties of the film and substrate on heating process of the film are quantitatively and rigorously provided.

2. Analytical model

In this study, a film on an semi-infinite substrate and a film of finite thickness s at initial temperature T_0 are subjected to energy transport from plasma, as illustrated in Fig. 1(a) and (b), respectively. The plasma comprised of the bulk plasma, presheath and sheath is in contact with an electrically negative bias wall partially reflecting or secondly emitting ions and electrons. When a negative bias voltage is applied to the film, high plasma energy including the total energies of the ions and electrons incident on the front surface increases temperatures in the finite film and film on the substrate and readily results in solid–liquid transition. Conduction is removed by convection at the bottom surface of the finite film with heat transfer coefficient h_∞. The major assumptions made are as follows [4,16,17]:

1. The model is one-dimensional due to a thin thickness of the region considered.
2. The plasma energy flux incident on the front surface of the film is considered as a surface heat source.
3. The plasma is in a quasi-steady state. The incident plasma irradiance on the front surface of the finite film and film is independent of time, while heat transfer in the film and substrate is unsteady.
4. The transport processes in the plasma in contact with the workpiece surface can be modeled as those in the plasma between two parallel plates.
5. The presheath and sheath are imposed by a negligible magnetic field or a magnetic field in a direction parallel to the ion flow. As a result, the one-dimensional ion flow can be assured.
6. The workpiece surface is electrically biased.
7. The ionization rate is determined from the Emmert et al.'s model [18]. Thermionic and field emissions of ions and electrons are ignored.
8. The effects of neutral particles are ignored.
9. Ion and electron reflectivities are constant. The secondary emissions of ions and electrons can be included into the reflectivities [19].
10. The physical and thermal parameters of the film and substrate can be different. The parameters of the finite film are the same as the film on the substrate. Joule heat in the film and energy loss from thermal radiation are neglected.
11. The interface is in perfect thermal contact between the film and substrate.

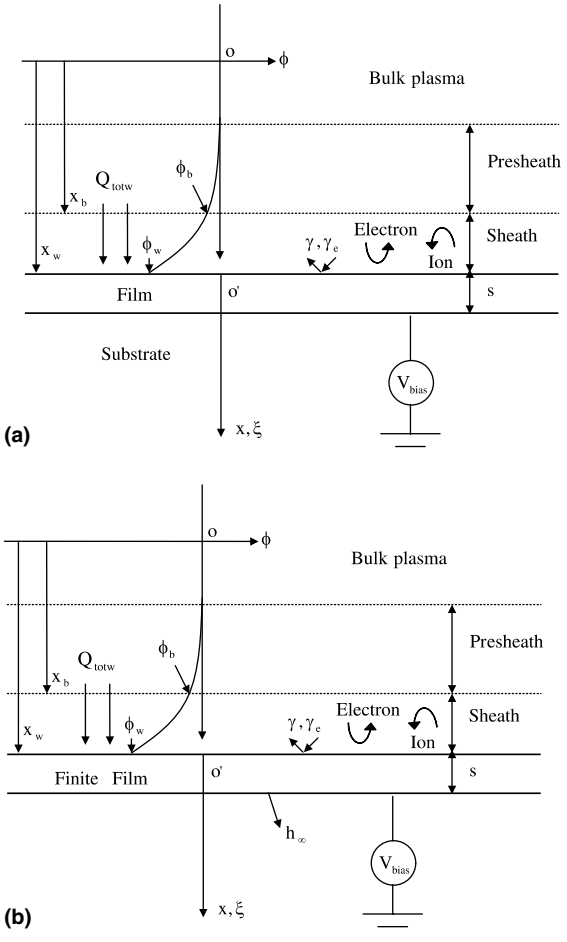

Fig. 1. Sketch for the physical model and coordinates: (a) a film on a substrate and (b) a finite film.

2.1. Plasma energy transport to film surface

The dimensionless plasma energy flux transport to the negative biased surface is given by [4]

$$Q_{\mathrm{totw}} = j_{\mathrm{iw}}\left(\Omega + \chi_{\mathrm{w}} - \chi_{\mathrm{b}} + \frac{E_{\mathrm{i}}}{Z_{\mathrm{i}}} - \varphi\right) + j_{\mathrm{ew}}(2+\varphi) \tag{1}$$

where function

$$\Omega \equiv \left[\frac{2}{Z_{\mathrm{i}}\kappa} - 1 + \frac{\sqrt{\chi_{\mathrm{b}}}}{D(\sqrt{\chi_{\mathrm{b}}})}\right] \tag{2}$$

The ion and electron current densities at the wall in Eq. (1) are, respectively,

$$j_{\mathrm{iw}} = j_{\mathrm{ib}} = \Omega_{1\mathrm{b}}\mathrm{e}^{-\chi_{\mathrm{b}}}, \quad j_{\mathrm{ew}} = (1-\gamma_{\mathrm{e}})\sqrt{\frac{M}{2\pi}}\mathrm{e}^{-\chi_{\mathrm{w}}} \tag{3}$$

where function

$$\Omega_{1\mathrm{b}} \equiv \frac{2(1-\gamma)}{1+\gamma}\sqrt{\frac{2}{Z_{\mathrm{i}}}}\frac{1+Z_{\mathrm{i}}\kappa}{\pi\kappa}\mathrm{e}^{\chi_{\mathrm{b}}}D(\sqrt{\chi_{\mathrm{b}}}) \tag{4}$$

where γ and γ_{e} denote the ion and electron reflectivity, respectively, Z_{i} is charge number and the dimensionless parameters κ and M are electron-to-ion source temperature ratio at presheath edge and ion-to-electron mass

ratio, respectively. Dimensionless energies E_i and φ are referred to ionization energy and work function, respectively. Dawson function $D(x)$ is defined in previous studies [17]. The sheath edge potential χ_b is satisfied by [17]

$$\frac{2}{\sqrt{\pi Z_i \kappa}} D(\sqrt{\chi_b}) = e^{Z_i \kappa \chi_b} \mathrm{erfc}(\sqrt{Z_i \kappa \chi_b}) \tag{5}$$

where function erfc(x) is the complementary error function [17]. The dimensionless wall potential yields [4]

$$\chi_w = \chi_{bias} + \chi_f = \chi_{bias} + \chi_b + \ln\left(\frac{1-\gamma_e}{\Omega_{1b}}\sqrt{\frac{M}{2\pi}}\right) \tag{6}$$

Differentiating Eq. (1) with χ_{bias} leads to

$$\frac{\partial Q_{totw}}{\partial \chi_{bias}} = j_{iw} - j_{ew}(2+\varphi) \tag{7}$$

Increasing of the bias voltage, the slope of total plasma energy flux versus bias voltage changes from negative to positive value [4]. The total plasma energy flux exhibits a minimum. When $\chi_{bias} \gg 0$, $j_{ew} \to 0$, Eq. (7) can be simplified to

$$\frac{\partial Q_{totw}}{\partial \chi_{bias}} = j_{iw} \tag{8}$$

which shows that the total plasma energy flux is linearly dependent on the bias voltage.

2.2. Plasma heating of a film on the substrate

The one-dimensional, unsteady heat conduction equations for the film and substrate in dimensionless forms, respectively, yield

$$\frac{\partial \lambda_f(\xi,\tau)}{\partial \tau} = \alpha_f \frac{\partial^2 \lambda_f(\xi,\tau)}{\partial \xi^2} \tag{9}$$

$$\frac{\partial \lambda_s(\xi,\tau)}{\partial \tau} = K_{sf}\rho_{fs}C_{pfs}\frac{\partial^2 \lambda_s(\xi,\tau)}{\partial \xi^2} \tag{10}$$

where the dimensionless thermal diffusivity $\alpha_f = 1$, the independent dimensionless parameters are defined as

$$C_{pfs} = \frac{c_{pf}}{c_{ps}}, \quad \rho_{fs} = \frac{\rho_f}{\rho_s}, \quad K_{sf} = \frac{k_s}{k_f} \tag{11}$$

The initial and boundary conditions for the film and substrate are, respectively,

$$\lambda_f(\xi,0) = 0, \quad \lambda_s(\xi,0) = 0 \tag{12}$$

$$-\frac{\partial \lambda_f(0,\tau)}{\partial \xi} = \Theta Q_{totw} \tag{13}$$

$$-\frac{\partial \lambda_f(1,\tau)}{\partial \xi} = -K_{sf}\frac{\partial \lambda_s(1,\tau)}{\partial \xi}, \quad \lambda_f(1,\tau) = \lambda_s(1,\tau) \tag{14}$$

$$\lambda_s(\infty,\tau) = 0 \tag{15}$$

where dimensionless parameter Θ represents the ratio between plasma flow work and heat conduction into the film. Substituting the initial conditions from Eq. (12), taking the Laplace transform with respect to time for Eqs. (9), (10) and (13)–(15), solutions of Eqs. (9) and (10) yield [20]

$$\lambda_f(\xi,\tau) = \sum_{n=0}^{\infty} \Theta Q_{totw} B^{n+1}\left\{2\sqrt{\frac{\tau}{\pi}}e^{-\frac{[2(n+1)-\xi]^2}{4\tau}} - [2(n+1)-\xi] \times \mathrm{erfc}\left[\frac{2(n+1)-\xi}{2\sqrt{\tau}}\right]\right\} + \sum_{n=0}^{\infty} \Theta Q_{totw} B^n \left[2\sqrt{\frac{\tau}{\pi}}e^{-\frac{(2n+\xi)^2}{4\tau}} - (2n+\xi)\mathrm{erfc}\left(\frac{2n+\xi}{2\sqrt{\tau}}\right)\right] \tag{16}$$

$$\lambda_s(\xi,\tau) = \sum_{n=0}^{\infty} 2\Theta Q_{totw}\frac{B^n}{(1+\varepsilon)}\left\{2\sqrt{\frac{\tau}{\pi}}e^{-\frac{\left[(\xi-1)\sqrt{\frac{1}{k_{sf}\rho_{fs}C_{pfs}}}+(2n+1)\right]^2}{4\tau}} - \left[(\xi-1)\sqrt{\frac{1}{k_{sf}\rho_{fs}C_{pfs}}}+(2n+1)\right] \times \mathrm{erfc}\left[\frac{(\xi-1)\sqrt{\frac{1}{k_{sf}\rho_{fs}C_{pfs}}}+(2n+1)}{2\sqrt{\tau}}\right]\right\} \tag{17}$$

where

$$B = \frac{1-\varepsilon}{1+\varepsilon}, \quad \varepsilon = \sqrt{\frac{K_{sf}}{\rho_{fs}C_{pfs}}} \tag{18}$$

Substituting $\xi = 0$ in Eq. (16), the dimensionless temperature of the front surface is found to be

$$\lambda_f(0,\tau) = 2\Theta Q_{totw}\sum_{n=0}^{\infty}\left\{B^{n+1}\left[\sqrt{\frac{\tau}{\pi}}e^{-\frac{(n+1)^2}{\tau}} - (n+1)\mathrm{erfc}\left(\frac{n+1}{\sqrt{\tau}}\right)\right] + B^n\left[\sqrt{\frac{\tau}{\pi}}e^{-\frac{n^2}{\tau}} - n\mathrm{erfc}\left(\frac{n}{\sqrt{\tau}}\right)\right]\right\} \tag{19}$$

The critical time τ_m required to initiate melting on the front surface is determined when $\lambda_f(0,\tau)$ is identical to λ_{fm}. The effects of various processing parameters on the critical time for onset of melting at the front surface are determined from Eq. (19). The heating rate at the front surface of the film is

$$\frac{\partial \lambda_f(0,\tau)}{\partial \tau} = \frac{\Theta Q_{totw}}{\sqrt{\pi\tau}}\sum_{n=0}^{\infty}[B^{n+1}e^{-\frac{(n+1)^2}{\tau}} + B^n e^{-\frac{n^2}{\tau}}] \tag{20}$$

The dimensionless temperature at the interface between the film and substrate is determined by substituting $\xi = 1$ in Eq. (16). This gives

$$\lambda_f(1,\tau) = \Theta Q_{totw}\sum_{n=0}^{\infty} B^n(B+1)\left[2\sqrt{\frac{\tau}{\pi}}e^{-\frac{(2n+1)^2}{4\tau}} - (2n+1)\mathrm{erfc}\left(\frac{2n+1}{2\sqrt{\tau}}\right)\right] \tag{21}$$

The heat flux at the bottom surface of the film is

$$-\frac{\partial\lambda_{\mathrm{f}}(1,\tau)}{\partial\xi}=\Theta Q_{\mathrm{totw}}\sum_{n=0}^{\infty}B^{n}(1-B)\mathrm{erfc}\left(\frac{2n+1}{2\sqrt{\tau}}\right) \tag{22}$$

Thermal analysis of the substrate can be avoided if contact Biot number $Bi_{\mathrm{c}}=h_{\mathrm{c}}s/k_{\mathrm{f}}$, where h_{c} denotes contact heat transfer coefficient, is introduced. Heat flux therefore can be evaluated by

$$-\frac{\partial\lambda_{\mathrm{f}}(1,\tau)}{\partial\xi}=Bi_{\mathrm{c}}\lambda_{\mathrm{f}}(1,\tau) \tag{23}$$

The contact Biot number Bi_{c} is obtained by substituting Eqs. (21) and (22) into Eq. (23). That is,

$$Bi_{\mathrm{c}}=\frac{\varepsilon\sum_{n=0}^{\infty}B^{n}\mathrm{erfc}(\frac{2n+1}{2\sqrt{\tau}})}{\sum_{n=0}^{\infty}B^{n}\left[2\sqrt{\frac{\tau}{\pi}}\mathrm{e}^{-\frac{(2n+1)^{2}}{4\tau}}-(2n+1)\mathrm{erfc}\left(\frac{2n+1}{2\sqrt{\tau}}\right)\right]} \tag{24}$$

The variation of temperature with time in the film on the substrate therefore can be calculated by solely solving the heat conduction equation of the film using the contact Biot number.

2.3. Plasma heating of a finite film

The unsteady, one-dimensional heat conduction equation in a dimensionless form for the finite film is

$$\frac{\partial\lambda_{\mathrm{ff}}(\xi,\tau)}{\partial\tau}=\alpha_{\mathrm{ff}}\frac{\partial^{2}\lambda_{\mathrm{ff}}(\xi,\tau)}{\partial\xi^{2}} \tag{25}$$

where the dimensionless thermal diffusivity $\alpha_{\mathrm{ff}}=1$, the initial and boundary conditions for the finite film are, respectively,

$$\lambda_{\mathrm{ff}}(\xi,0)=0 \tag{26}$$

$$-\frac{\partial\lambda_{\mathrm{ff}}(0,\tau)}{\partial\xi}=\Theta Q_{\mathrm{totw}} \tag{27}$$

$$-\frac{\partial\lambda_{\mathrm{ff}}(1,\tau)}{\partial\xi}=Bi\lambda_{\mathrm{ff}}(1,\tau) \tag{28}$$

The solution of Eq. (25) is found to be [21]

$$\lambda_{\mathrm{ff}}(\xi,\tau)=-\Theta Q_{\mathrm{totw}}\xi+\Theta Q_{\mathrm{totw}}+\frac{\Theta Q_{\mathrm{totw}}}{Bi}-2\Theta Q_{\mathrm{totw}}\sum_{m=1}^{\infty}\mathrm{e}^{-\beta_{\mathrm{m}}^{2}\tau}\frac{(\beta_{\mathrm{m}}^{2}+Bi^{2})\cos\beta_{\mathrm{m}}\xi}{\beta_{\mathrm{m}}^{2}[(\beta_{\mathrm{m}}^{2}+Bi^{2})+Bi]} \tag{29}$$

The variables of β_{m} are eigenvalues satisfied by $\tan\beta_{\mathrm{m}}=Bi/\beta_{\mathrm{m}}$. The dimensionless temperature on the front surface of the finite film yields

$$\lambda_{\mathrm{ff}}(0,\tau)=\Theta Q_{\mathrm{totw}}+\frac{\Theta Q_{\mathrm{totw}}}{Bi}-2\Theta Q_{\mathrm{totw}}\sum_{m=1}^{\infty}\mathrm{e}^{-\beta_{\mathrm{m}}^{2}\tau}\times\frac{(\beta_{\mathrm{m}}^{2}+Bi^{2})}{\beta_{\mathrm{m}}^{2}[(\beta_{\mathrm{m}}^{2}+Bi^{2})+Bi]} \tag{30}$$

The heating rate of the front surface of finite film is

$$\frac{\partial\lambda_{\mathrm{ff}}(0,\tau)}{\partial\tau}=2\beta_{\mathrm{m}}^{2}\Theta Q_{\mathrm{totw}}\sum_{m=1}^{\infty}\mathrm{e}^{-\beta_{\mathrm{m}}^{2}\tau}\frac{(\beta_{\mathrm{m}}^{2}+Bi^{2})}{\beta_{\mathrm{m}}^{2}[(\beta_{\mathrm{m}}^{2}+Bi^{2})+Bi]} \tag{31}$$

When $\tau_{\mathrm{m}}\to\infty$, we obtain the minimum Biot number required to prevent from melting at the front surface from Eq. (30). This gives

$$Bi=\frac{\Theta Q_{\mathrm{totw}}}{\lambda_{\mathrm{ffm}}-\Theta Q_{\mathrm{totw}}} \tag{32}$$

Differentiating Eq. (32) with χ_{bias} and invoking Eq. (8) lead to

$$\frac{\partial Bi}{\partial\chi_{\mathrm{bias}}}=\frac{\lambda_{\mathrm{ffm}}\Theta j_{\mathrm{iw}}}{(\lambda_{\mathrm{ffm}}-\Theta Q_{\mathrm{totw}})^{2}} \tag{33}$$

which indicates that the Biot number increases with bias voltage for $\chi_{\mathrm{bias}}\gg 0$. It is interesting to find the relationship between the heat flux at the interface between the film and substrate and that at the bottom of the finite film. The artificial Biot number, $Bi_{\mathrm{a}}=h_{\mathrm{a}}s/k_{\mathrm{f}}$, where h_{a} denotes an artificial heat transfer coefficient between the film and substrate, is introduced to simulate the Biot number of the finite film. The heat conduction flux at the bottom of the finite film is equal to that at the interface between the film and substrate.

$$Bi\lambda_{\mathrm{ff}}(1,\tau)=Bi_{\mathrm{a}}\lambda_{\mathrm{f}}(1,\tau) \tag{34}$$

Substituting Eqs. (21) and (29) at $\xi=1$ into Eq. (34), the artificial Biot number is found to be

$$Bi_{\mathrm{a}}=\frac{1-2Bi\sum_{m=1}^{\infty}\mathrm{e}^{-\beta_{\mathrm{m}}^{2}\tau}\frac{(\beta_{\mathrm{m}}^{2}+Bi^{2})\cos\beta_{\mathrm{m}}}{\beta_{\mathrm{m}}^{2}[(\beta_{\mathrm{m}}^{2}+Bi^{2})+Bi]}}{\sum_{n=0}^{\infty}B^{n}(B+1)\left[2\sqrt{\frac{\tau}{\pi}}\mathrm{e}^{-\frac{(2n+1)^{2}}{4\tau}}-(2n+1)\mathrm{erfc}\left(\frac{2n+1}{2\sqrt{\tau}}\right)\right]} \tag{35}$$

3. Results and discussion

To confirm relevancy and accuracy of this model, a comparison between the predicted and measured surface temperature as a function of time [22] for a nitrogen plasma and silicon wafer is shown in Fig. 2. In this case, the referenced data for comparison are listed in Table 1. The predicted temperature as a function of time agrees quite well with experimental data [22]. The deviation in the predicted temperature being higher and lower than the experimental data before and after 160 s, respectively, can be due to the consideration of plasma energy as a surface heat source in our model. In reality, the ions of nitrogen penetrate into the film and release recombination energy at some distance below the surface.

The effects of ion and electron reflectivities, charge number, ion-to-electron mass ratio, and electron-to-ion

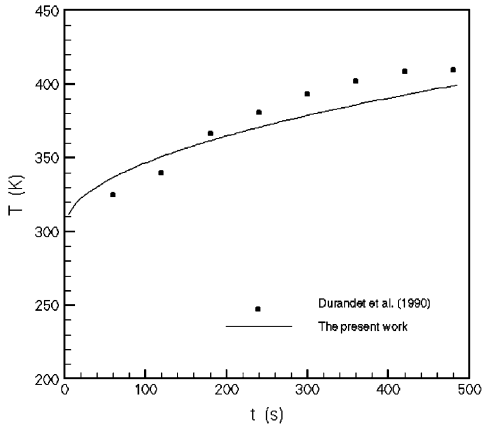

Fig. 2. Comparisons of predicted dimensional temperature on the front surface of a film on a substrate versus dimensional time between this work and the results from Durandet et al. [22].

Table 1
Values of the data (nitrogen plasma, silicon film and aluminum substrate) for comparison with experimental data [22]

γ	0
γ_e	0
M	25,686
Z_i	1
κ	0.1
ϕ_{bias}	118 V
c_{pf} (Si)	700 J/kg K
c_{ps} (Al)	896 J/kg K
T_0, T_∞	300 K
k_f (Si)	150 W/m K
k_s (Al)	238 W/m K
ρ_f (Si)	2330 kg/m^3
ρ_s (Al)	2700 kg/m^3
s	0.01 m
n_{e0}	4×10^{17} m^{-3}
m_i	2.34×10^{-26} kg
T_{e0}	2×10^{4} K
E_i	14.6 eV
φ	4 eV

source temperature ratio at the presheath edge on dimensionless temperature profile in the film and substrate at the dimensionless time $\tau = 7$ are presented in Fig. 3(a). The dashed lines are the predicted results based on the referenced dimensionless parameters from Table 2, which are estimated from the data for a hydrogen plasma, aluminum film and glass substrate. Different lines specified by different values of dimensionless parameters represent these parameters being different from those of the referenced parameters. Symbols and their values in the legend are referred to the dashed line. In the case of the referenced case, it can be seen that the dimensionless temperature profile in the film gradually

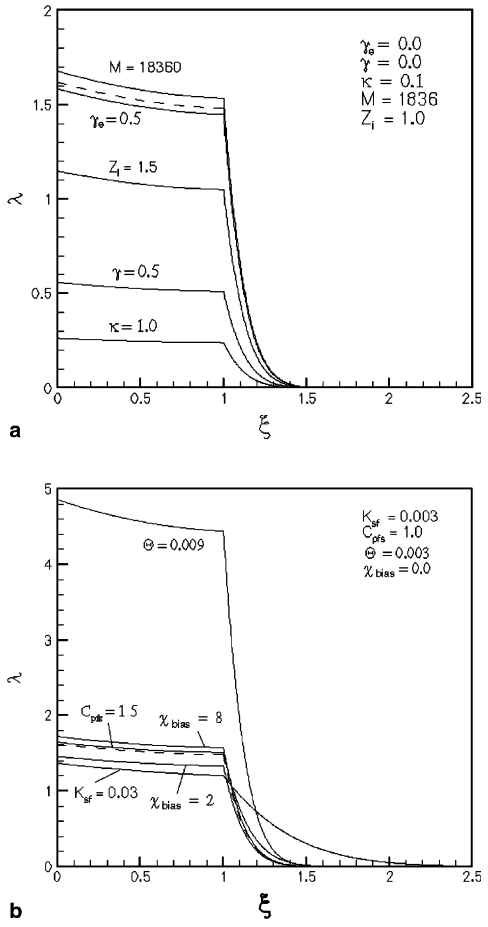

Fig. 3. Spatial variation of dimensionless temperature profiles in the film and substrate affected by: (a) reflectivities of ions and electrons, ion-to-electron mass ratio, charge number, and electron-to-ion source temperature ratio and (b) dimensionless bias voltage, substrate-to-film solid thermal conductivity ratio, film-to-substrate solid specific heat ratio, and plasma flow work-to-heat conduction ratio; dashed lines are based on Table 2.

Table 2
Values of the referenced dimensionless parameters

γ	0
γ_e	0
M	1836
Z_i	1
κ	0.1
E_i	8.0
φ	4.0
χ_{bias}	0
Θ	0.003
K_{sf}	0.003
ρ_{fs}	1
C_{pfs}	1
λ_{fm}, λ_{ffm}	2
Bi	5×10^{-4}

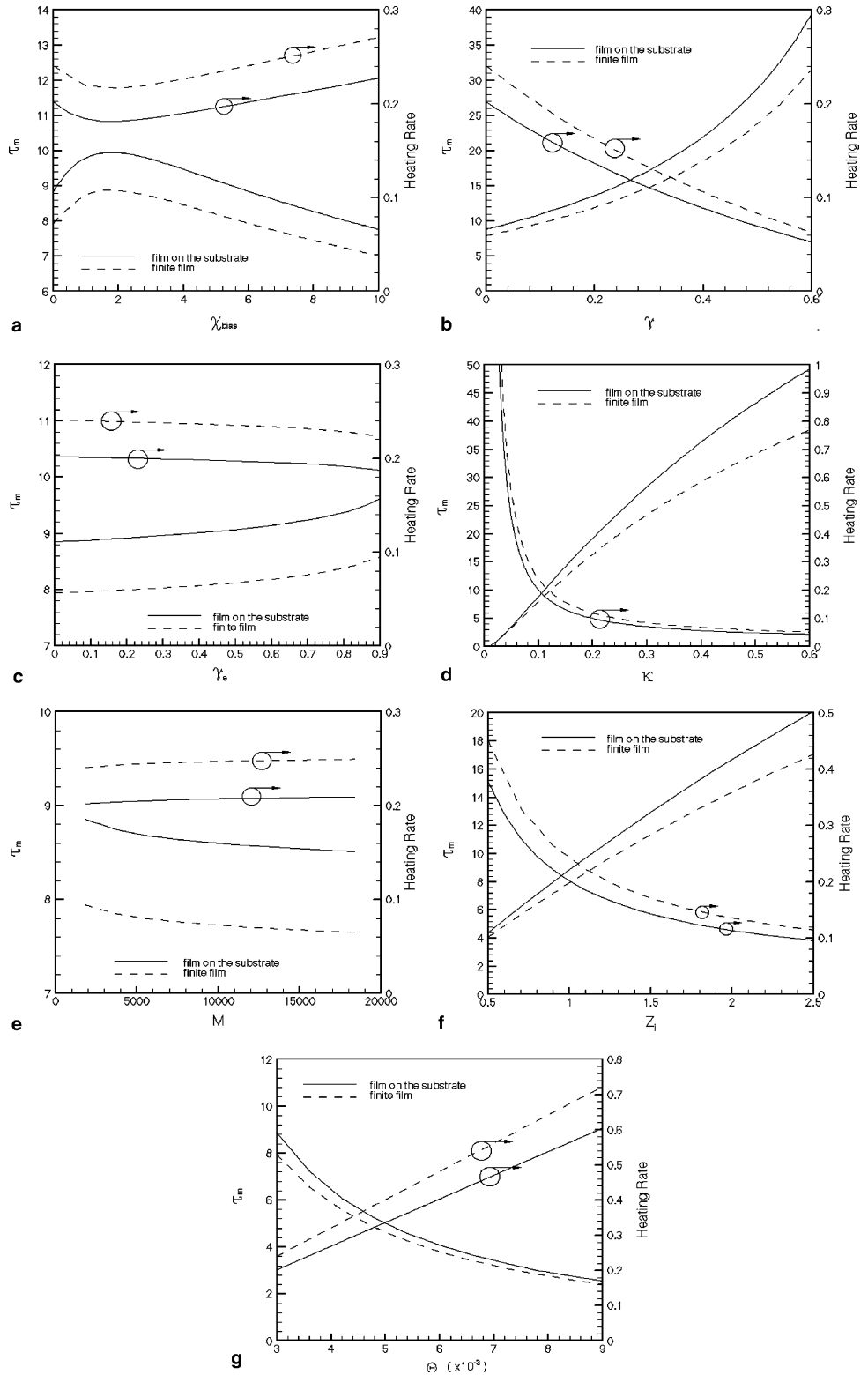

Fig. 4. Dimensionless melting time and heating rate at the front surface of the finite film and a film on the substrate affected by: (a) dimensionless bias voltage; (b) ions reflectivity; (c) electrons reflectivity; (d) electron-to-ion source temperature ratio at the presheath edge; (e) ion-to-electron mass ratio; (f) charge number and (g) plasma flow work-to-heat conduction ratio.

reduces in the forward direction from 1.62 to 1.48 (the temperature difference is about 42 K), but rapidly drops in the substrate. Except for ion-to-electron mass ratio, increasing of reflectivities of electrons and ions, charge number, and electron-to-ion source temperature ratio at the presheath edge result in decreasing of incident energy of plasma [4] and reducing the temperature profile in the film and substrate. The effects of dimensionless bias voltage, plasma flow work-to-heat conduction ratio, solid thermal conductivity ratio of substrate-to-film and specific heat ratio of film-to-substrate on the temperature profiles in the film and substrate at the $\tau = 7$ are shown in Fig. 3(b). The larger the thermal conductivity ratio of substrate-to-film, the quicker the heat is removed by conduction in the substrate. Hence, the temperature profile in the film is reduced and the penetrating depth of heat in the substrate is increased. Increasing of plasma flow work-to-heat conduction ratio and specific heat ratio of film-to-substrate result in increasing of the temperature in the film. The former is due to that the incident energy of plasma increases with plasma flow work-to-heat conduction ratio. The latter is a result of less heat flux from the film to substrate due to the higher temperature in the substrate. Because of the larger the film-to-substrate specific heat ratio, less energy is required to heat the substrate per degree of temperature. The variation of plasma energy with dimensionless bias voltage has a minimum between 0 and 8, as can be seen in [4] (or see Eq. (7)). Hence, the temperature in the film decreases and increases at bias voltage of 2 and 8, respectively.

Dimensionless melting time and heating rate at the front surface of a finite film and a film on the substrate as function of dimensionless bias voltage, ions and electrons reflectivities, electron-to-ion source temperature ratio at the presheath edge, ion-to-electron mass ratios, charge number and plasma flow work-to-heat conduction ratios are shown in Fig. 4(a)–(g), respectively. In these figures, the dashed and solid lines represent the finite film and the film on the substrate, respectively. The melting time and heating rate are calculated based on $\lambda_{fm} = \lambda_{ffm} = 2$ and $\tau = 10$, respectively. In Fig. 4(a), the floating wall potential corresponding to the dimensionless negative bias voltage is zero. The larger the dimensionless bias voltage, the more the ion and the less the electron energy transport to the surface, respectively. The heating rate on the front surface has a minimum and the melting time has a maximum in this bias voltage range. The melting time linearly decreases with increasing of bias voltage for higher bias voltage (see Eq. (8)). It is noted that the melting time and heating rate profiles of the finite film and film on the substrate are similar. Increasing of ion-to-electron mass ratios and decreasing of ions and electron reflectivities, electron-to-ion source temperature ratio and charge number result in increasing the plasma energy transport to surface [4]. The heating rate thus is higher and melting time is shorter. Increasing the plasma flow work-to-heat conduction ratio implies a higher heat conduction into the film (see Eqs. (13) and (27)) and shorter melting time. In the referenced case, the heating rate of the finite film is higher than that of the film on the substrate, resulting in the melting time of the former to be shorter than that of the latter.

Fig. 5(a) and (b) present dimensionless melting time and heating rate at the front surface of the film on the substrate as function of substrate-to-film solid thermal conductivity and film-to-substrate specific heat ratios, respectively. In Fig. 5(a), increasing of substrate-to-film solid thermal conductivity ratio implies that the cooling effect of conduction into the substrate on the front surface of film is strong. Hence, the heating rate and melting time is reduced and raised, respectively. It can be seen in Fig. 5(b), in contrast to substrate-to-film solid thermal conductivity ratio, increasing of film-to-substrate specific heat ratio represents that the effects of cooling of the substrate on the front surface of the film

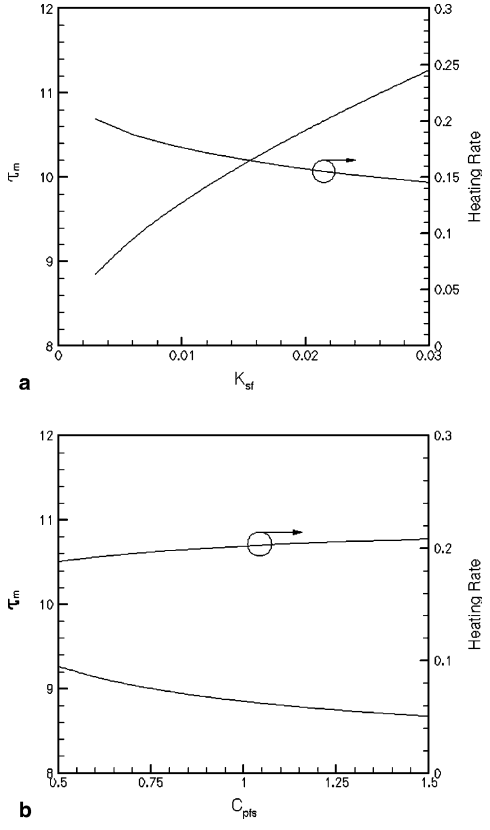

Fig. 5. Dimensionless melting time and heating rate at the front surface of a film on the substrate affected by: (a) substrate-to-film solid thermal conductivity ratio and (b) film-to-substrate solid specific heat ratio.

is weak. Hence, the heating rate and melting time is raised and reduced, respectively. Dimensionless melting time and heating rate at the front surface of the finite film as functions of Biot number are shown in Fig. 6. The higher the Biot number, the quicker the heat is removed by convection to the surrounding, resulting in the heating rate and melting time to be reduced and raised, respectively.

The contact Biot number versus dimensionless time affected by the substrate-to-film solid thermal conductivity and film-to-substrate specific heat ratios are presented in Fig. 7. The solid line is the predicted results based on the referenced dimensionless parameters from Table 2. The cooling effect of the substrate on the film is higher at the initial time, since the substrate temperature is at the ambient temperature. The contact Biot number rapidly drops at the initial time and then monotonically reduces. The latter is a result of the substrate

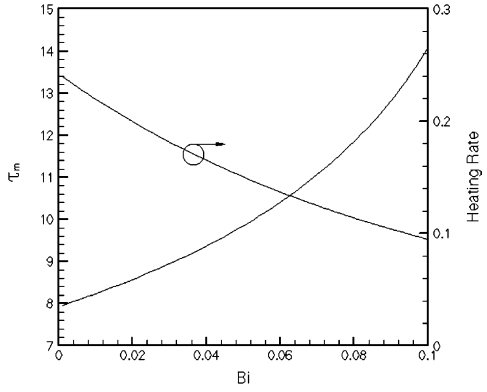

Fig. 6. Dimensionless melting time and heating rate at the front surface of the finite film as function of Biot number.

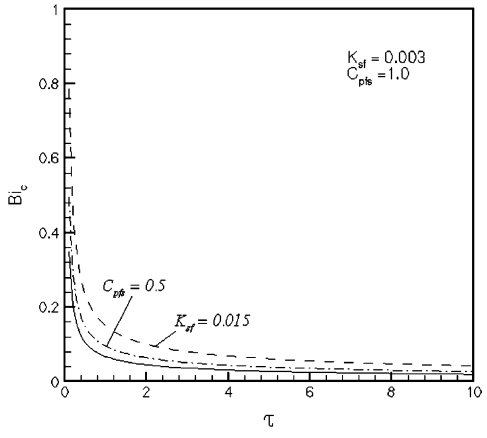

Fig. 7. The contact Biot number versus dimensionless time affected by substrate-to-film solid thermal conductivity ratio and film-to-substrate solid specific heat ratio; the solid line is based on Table 2.

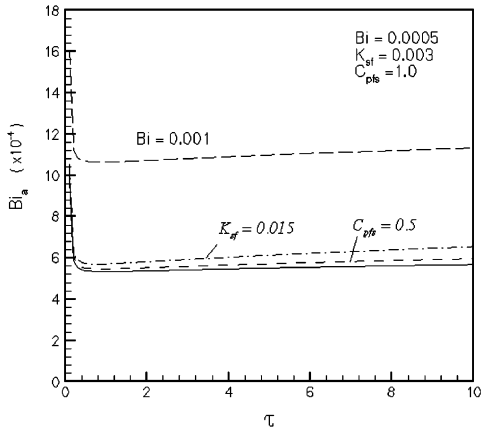

Fig. 8. The artificial Biot number versus dimensionless time affected by Biot number, substrate-to-film solid thermal conductivity ratio and film-to-substrate solid specific heat ratio; the solid line is based on Table 2.

temperature raising and the heat conduction flux between the film and substrate reducing. Increasing the substrate-to-film solid thermal conductivity ratio and decreasing film-to-substrate specific heat ratio indicate that the cooling effects of substrate on the film is higher, resulting in increasing of the contact Biot number.

The artificial Biot numbers versus dimensionless time affected by Biot number, substrate-to-film solid thermal conductivity ratio, and film-to-substrate solid specific heat ratio are shown in Fig. 8. The solid line is calculated based on Table 2. It can be seen on the solid line, the artificial Biot number rapidly drops from 9.8×10^{-4} to 5.33×10^{-4} for $\tau = 0.01$–1, and then monotonically increases to 5.67×10^{-4} at $\tau = 10$. The latter results from the increase of substrate temperature, because the artificial Biot number must be increased to enhance heat conduction flux between the film and substrate. In the dimensionless time considered, the artificial Biot number is larger than the Biot number, resulting in the heating rate of the finite film to be larger than that of the film on the substrate (it can be seen in Fig. 4(a)–(g)). An increasing of Biot number increases artificial Biot number. The effects of substrate-to-film solid thermal conductivity and film-to-substrate solid specific heat ratios on the artificial Biot number are same as the Fig. 7.

4. Conclusions

(1) Plasma heating of workpieces is important for plasma processing. It is crucial to control temperature of the workpieces to prevent from melting in the fusion devices and improve the ion diffusion rate in ion implantation process. An analytical solution is derived to calculate the melting time and heating rate of the front

surface of a film on a substrate with negative bias voltage in contact with a plasma. This work provides quantitative results applicable to control the temperature evolution and the melting time in the film. The effects of plasma parameters on heating rates and melting time in the film are found to be significant. The predicted surface temperature of the film on the substrate as function of time agrees well with experimental data. The results can be used to control temperature evolution and the melting time in the film by choosing appropriate process parameters.

(2) Temperature and heating rate of the front surface of the finite film and film on the substrate increase with increasing the ion-to-electron mass ratio, film-to-substrate specific heat ratio and plasma flow work-to-heat conduction ratio, and decreasing reflectivities of electrons and ions, charge number, electron-to-ion source temperature ratio at the presheath edge, substrate-to-film solid thermal conductivity ratio and Biot number. The total plasma energy flux at the wall and the melting time exhibit a minimum and a maximum values, respectively, in the bias voltage range considered. The dimensionless parameters are reversed to increase the melting time.

References

[1] F.F. Chen, Introduction to Plasma Physics, Plenum Press, New York, 1974.
[2] D. Bohm, Minimum ionic kinetic energy for a stable sheath, in: A. Guthrie, R. Wakerling (Eds.), The Characteristics of Electrical Discharges in Magnetic Fields, McGraw Hill, New York, 1949, pp. 77–86.
[3] H. Kersten, H. Deutsch, H. Steffen, G.M.W. Kroesen, R. Hippler, The energy balance at substrate surfaces during plasma processing, Vacuum 63 (2001) 385–431.
[4] F.B. Yeh, P.S. Wei, Plasma energy transport to an electrically biased surface, Int. J. Heat Mass Transfer 47 (2004) 4019–4029.
[5] P.C. Stangeby, Plasma sheath transmission factors for tokamak edge plasmas, Phys. Fluids 27 (1984) 682–690.
[6] M.S. Benilov, A. Marotta, A model of the cathode region of atmospheric pressure arcs, J. Phys. D: Appl. Phys. 28 (1995) 1869–1882.
[7] L. Costanzo, J.P. Gunn, T. Loarer, L. Colas, Y. Corre, P.H. Ghendrih, C. Grisolia, A. Grosman, D. Guilhem, P. Monier-Garbet, R. Reichle, H. Roche, J.C. Vallet, Analysis of energy flux deposition and sheath transmission factors during ergodic divertor operation on tore supra, J. Nucl. Mater. 290–293 (2001) 840–844.
[8] S. Mändl, D. Manova, B. Rauschenbach, Balancing incident heat and ion flow for process optimization in plasma based ion implantation, J. Phys. D: Appl. Phys. 35 (2002) 1141–1148.
[9] H. Schmitz, K.-U. Riemann, Analysis of the cathodic region of atmospheric pressure discharges, J. Phys. D: Appl. Phys. 35 (2002) 1727–1735.
[10] S. Masuzaki, N. Ohno, S. Takamura, Experimental study on plasma heat flow to plasma-facing materials, J. Nucl. Mater. 223 (1995) 286–293.
[11] S. Takamura, M.Y. Ye, T. Kuwabara, N. Ohno, Heat flows through plasma sheaths, Phys. Plasmas 5 (1998) 2151–2158.
[12] M. Araki, M. Kobayashi, High-speed surface temperature measurements on plasma facing materials for fusion applications, Rev. Sci. Instrum. 67 (1996) 178–184.
[13] A.R. Raffray, G. Federici, RACLETTE: a model for evaluating the thermal response of plasma facing components to slow high power plasma transients. Part I: Theory and description of model capabilities, J. Nucl. Mater. 244 (1997) 85–100.
[14] K. Takaki, A. Takahashi, T. Fujiwara, Experimental study on heat flux from an argon RF plasma using laser interferometry method, Jpn. J. Appl. Phys. 37 (1998) 3514–3520.
[15] J.P. Blanchard, Target temperature prediction for plasma source ion implantation, J. Vac. Sci. Technol. B 12 (1994) 910–917.
[16] F.B. Yeh, P.S. Wei, Effects of plasma parameters on the temperature field in a workpiece experiencing solid–liquid phase transition, ASME J. Heat Transfer 127 (2005), in press.
[17] P.S. Wei, F.B. Yeh, Fluid-like transport variables in a kinetic, collisionless plasma near a surface with ion and electron reflection, IEEE Trans. Plasma Sci. 28 (2000) 1233–1243.
[18] G.A. Emmert, R.M. Wieland, A.T. Mense, J.N. Davidson, Electric sheath and presheath in a collisionless, finite ion temperature plasma, Phys. Fluids 23 (1980) 803–812.
[19] P.C. Stangeby, The plasma sheath, in: D.E. Post, R. Behrisch (Eds.), Physics of plasma wall interactions in controlled fusion, Proceedings of NATO Advanced Study Institute, 30 July–10 August 1984, Val-Morin, Quebec, Canada, Plenum, New York, 1986, pp. 41–97.
[20] M.K. El-Adawi, M.A. Abdel-Naby, S.A. Shalaby, Laser heating of a two-layer system with constant surface absorption: an exact solution, Int. J. Heat Mass Transfer 38 (1993) 947–952.
[21] M.N. Özisik, Heat Conduction, Wiley, New York, 1993.
[22] A. Durandet, O. Joubert, J. Pelietier, M. Pichot, Effects of ion bombardment and chemical reaction on wafer temperature during plasma etching, J. Appl. Phys. 67 (1990) 3862–3866.